




# Experimental and numerical studies on the deformation response and retaining mechanism of h-type anti-sliding piles in clay landslide

Xin-Rong Liu<sup>1,2</sup> · Miao-Miao Kou<sup>1,2</sup>  · Hao Feng<sup>1,2</sup> · Yang Zhou<sup>1,3</sup>

Received: 24 July 2017 / Accepted: 18 February 2018 / Published online: 23 February 2018  
© Springer-Verlag GmbH Germany, part of Springer Nature 2018

## Abstract

This paper performs systematical studies on deformation response and retaining mechanism of a novel retaining structure, i.e., an h-type anti-sliding pile, which has been used to stabilize slopes in mountain areas. The present systematical studies can be divided into two parts, including experimental studies and numerical investigations. Firstly, the physical scale model tests are conducted to study the effect of anchor depths on distributions of sliding thrust and resistant forces on the h-type anti-sliding pile in clay landslides. Four kinds of h-type anti-slide piles with different anchor depths are tested in the physical scale clay slope subjected to static loads. Secondly, the above four physical models are simulated using finite element method. The numerical results are in good agreement with the experimental data, which prove the ability and accuracy of the present numerical simulations. In addition, several different numerical models are performed to investigate the effects of sliding surface angles, crossbeam lengths and different anchor depths on the deformation response and retaining mechanism of h-type anti-slide piles in the clay slope under static loads. It can be found from experimental and numerical results that deformation responses and retaining mechanism of h-type anti-sliding piles are not only related to sliding surface angles, but also related to crossbeam lengths and anchor depths. Finally, some design suggestions of h-type anti-slide piles are proposed based on the experimental and numerical studies. This work is expected to improve understanding of h-type anti-slide piles in clay landslide and to provide some references to engineers in design.

**Keywords** Slope stabilization · h-Type anti-sliding pile · Anchor depths · Sliding surface angles · Crossbeam lengths

## Introduction

Landslides can be regarded as a kind of significant geotechnical hazard in Southwest China, which may threaten many people. Due to harmfulness of landslides, a number of slope stabilization instruments, such as anti-sliding piles, retaining walls, soil nailing, benching and anchor bolts, are developed

to prevent the potential natural hazards (Abramson et al. 2002; Usluogullari et al. 2016).

Compared with other retaining wall instruments, which require more spaces, anti-sliding piles are widely applied to stabilize slopes in many cases (Ito and Matsui 1975; Poulos 1995; Kourkoulis et al. 2011; Song et al. 2012; Tang et al. 2014; Usluogullari et al. 2016) to control landslides. The anti-sliding piles play an important role in maintaining the stability of slopes by transferring body and shear forces from the landslide mass to underlying stable layers. Different types of anti-sliding piles have been developed, including common anti-sliding pile, anchored anti-sliding pile and combination anti-sliding pile, based on different landslide geological conditions, landslide scales and project requirements.

The distribution of sliding thrust forces and resistant forces on anti-sliding piles in landslides is a key factor in the design. A few decades ago, many researches were conducted to investigate the distribution of sliding thrust forces and resistant forces on the common anti-sliding piles, which

**Electronic supplementary material** The online version of this article (<https://doi.org/10.1007/s12665-018-7360-3>) contains supplementary material, which is available to authorized users.

✉ Miao-Miao Kou  
koumiaomiao19890219@yeah.net

<sup>1</sup> School of Civil Engineering, Chongqing University, Chongqing 400045, People's Republic of China

<sup>2</sup> Key Laboratory of New Technology for Construction of Cities in Mountain Area, Chongqing University, Chongqing 400045, People's Republic of China

<sup>3</sup> Chengdu Engineering Corporation Limited, Chengdu 610000, People's Republic of China

are the most widely used in slopes. Previous studies on the distributions of the sliding thrust forces and resistant forces show that soil pressure along the vertical direction may assume triangular, rectangular, sigmoidal, parabolic shapes, or some combination of them (Ito et al. 1981; Hassiotis et al. 1997; Li et al. 2013). Xu et al. (1988a, b, 1990) concluded that the soil pressure distribution is assumed as triangular shapes using the physical experimental tests in the loose sand or clay based on the field tests. However, the basic rectangular distribution of soil pressure on anti-sliding piles was assumed in the deep-buried anti-sliding piles in sliding masses by Xiong (2000). In addition, some other researchers found parabolic soil pressure distributions during field monitoring, laboratory tests and numerical simulations (Liu and Yu 1984; Xiao 2010; Zheng and Zhao 2004; Jiao et al. 2013). Kim and Kim (1999) quantified different effects on the behavior of laterally loaded single piles by model tests. Dai (2002), Yang et al. (2006) and Wang et al. (2010) deduced an analytical expression and computational method to determine the form of the forces on the anti-sliding piles for landslide soil pressures corresponding to triangular, rectangular, and parabola shapes.

Although the common anti-sliding piles are widely applied in terms of controlling stabilization of slopes, an obvious stress concentration effect occurs near sliding surface. In order to optimize stress concentration and improve the retaining performance of anti-sliding piles, the combination anti-sliding pile is formed by the rigid combination of two or more rows of common anti-sliding piles (Zhao et al. 2017). The combination anti-sliding piles are frequently used in the southwest mountain areas of China (Wang 2011). Moreover, due to the large scale of landslides, a single common anti-sliding pile or arrays of common anti-sliding piles cannot satisfy the resistant forces in landslides (Cornforth 2005), and engineering experiences show that the cost is very high when the common anti-sliding piles are used to treat large size landslides (Zhao et al. 2017).

Recently, a novel retaining structure, namely h-type anti-sliding pile, was designed and constructed to treat landslides along the Chuan-Yun railway in southwest areas of China. On the basis of double-row anti-sliding piles (Wang and Zhou 2011), h-type anti-sliding pile consists of front pile, back pile and crossbeam. In recent years, h-type anti-sliding piles have been widely used to control landslides in the southwest mountain region (Zhao et al. 2017). However, only a few scholars have conducted researches on the h-type anti-sliding piles in landslides (Ou et al. 2012; Xiao 2010; Zhao et al. 2017). The previous studies mainly focused on the monitoring data of h-type anti-sliding piles in the field tests and engineering projects. The mechanism of h-type anti-sliding piles in landslides is still needed to be systematically investigated. Therefore, understandings of deformation

response and retaining mechanism of h-type anti-sliding piles are required.

The main objective of this work is to develop the understanding of deformation responses and retaining mechanism of h-type anti-sliding pile in the clay landslide models with different design parameters. In order to achieve this objective, the physical scale model tests of an h-type anti-sliding pile in clay landslide models under static loads are conducted in this work. The sliding thrust and resistant pressures on the back and front piles of h-type anti-sliding piles are measured by the soil pressure cells installed on the anti-sliding piles. The influence of anchor depth in h-type anti-sliding piles on the sliding thrust and resistant pressure is studied in the physical scale model tests. Moreover, the similar numerical examples of h-type anti-sliding piles in clay landslides are simulated using finite element method (FEM). The numerical results are compared with the experimental data, which illustrates the effectiveness of numerical simulations. Furthermore, in order to study other design parameters, such as sliding surface angle, crossbeam length and different anchor depth, on the deformation response and retaining mechanism of h-type anti-sliding piles in landslides, several numerical examples are modeled by FEM. Some rules of sliding thrust and resistant pressures on the front and back piles are concluded, and some suggestions about application of h-type anti-sliding piles in the clay slopes are provided based on the experimental and numerical results.

This paper is organized as follows. “[Experimental and numerical methodologies](#)” are described in second section. “[Experimental results](#)” are shown in third section. “[Numerical results and discussions](#)” are performed in fourth section. “[Conclusions](#)” are drawn in fifth section.

## Methodology

### Experimental method

#### Landslide model preparation

An approximate landslide physical model used in experiments must have the similar behaviors to a real landslide (Tang et al. 2014). Based on works by Yang (2005), the physical model should be dynamically similar to the actual landslide in terms of its geometry, physical parameters, initial state, and boundary conditions.

As shown in Fig. 1a, the present physical landslide model tests consist of sliding bed, sliding surface, sliding masses and an h-type anti-sliding pile. The models are 900 mm in length, 400 mm in width and 1000 mm in height (Fig. 1a). The sliding surface angle is a 15° inclined plane, and the slope inclined angle is 45°. It can be found from Figure S1a

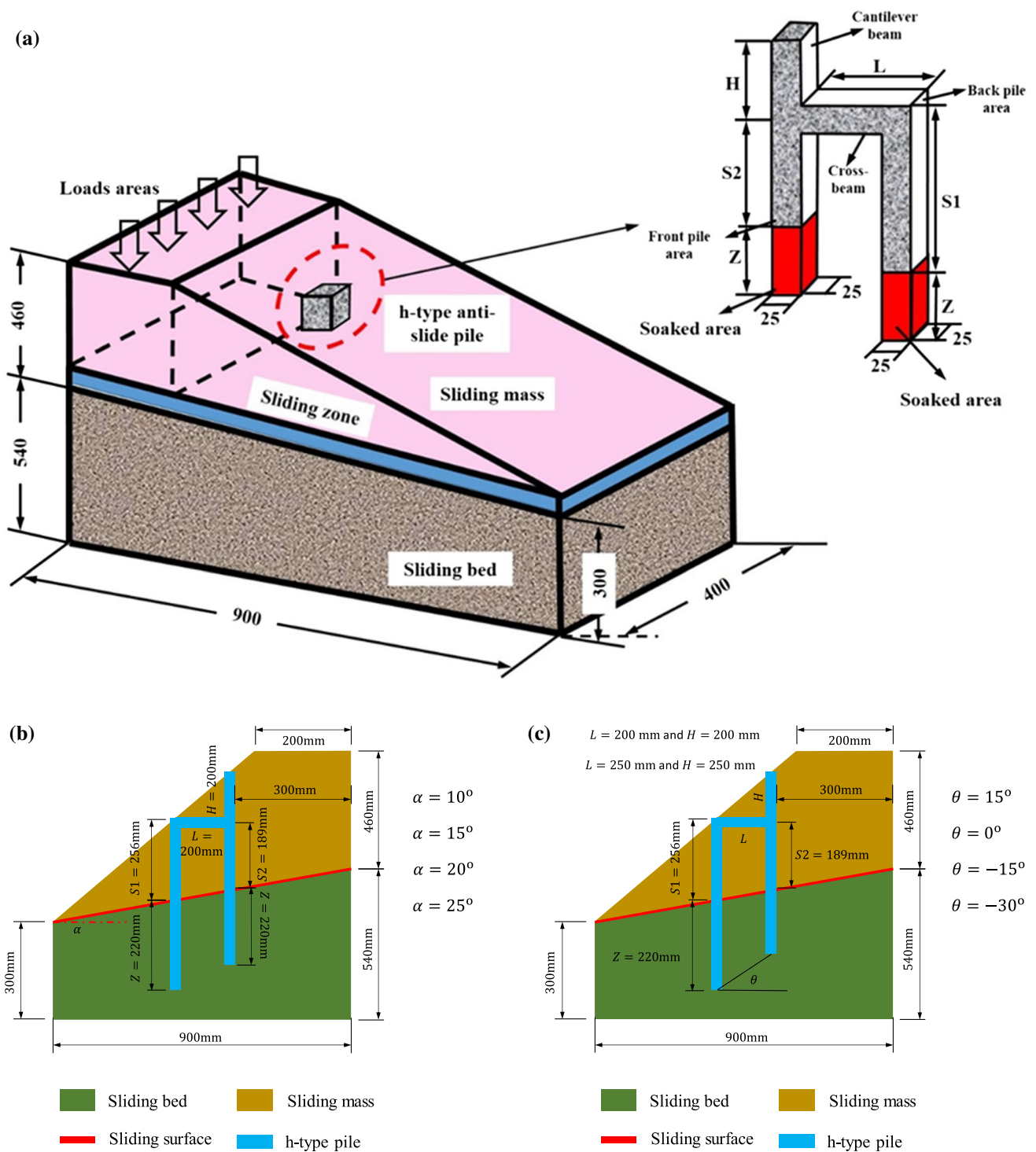


**Fig. 1** a Schematics of physical landslide model (Unit: mm), b geometry of landslide models with different sliding surface angles and c geometry of landslide models with different anchor depth between front and back piles in an h-type pile

in the Supplementary Electronic Materials that the model frames were welded by steel.

Based on the previous works by Yang (2005), Zhao et al. (2017), Li et al. (2017), Tang et al. (2014) Xiang et al. (2015), the rectangular sections with  $25 \times 25 \text{ mm}^2$  are

employed in the anti-sliding piles. The h-type anti-sliding pile is taken as hollow steel tube. In h-type anti-sliding piles, anchor depth is denoted as  $Z$ , crossbeam length is denoted  $L$ , cantilever beam length is represented as  $H$ , length between sliding surface and crossbeam in the front pile is labeled as

**Table 1** Mechanical properties of soil in sliding mass

Moisture content (%)	Unit weight (kN/m <sup>3</sup> )	Young's modulus (MPa)	Poisson's ratio	Cohesive strength (kPa)	Frictional angle (°)
16.3	18.50	6.0	0.3	48.6	19.8

**Table 2** Mechanical properties of soil in sliding bed

Moisture content (%)	Unit weight (kN/m <sup>3</sup> )	Young's modulus (MPa)	Poisson's ratio	Cohesive strength (kPa)	Frictional angle (°)
12.6	19.86	8.0	0.25	57.5	23.5

$S_2$  and that between sliding surface and crossbeam in the back pile is marked as  $S_1$ , which are plotted in Fig. 1a. The material of an h-type anti-sliding pile is steel. The average mechanical parameters of the h-type anti-sliding pile are listed as follow: Young's modulus  $E = 206$  GPa, Poisson's ratio  $\nu = 0.2$  and mass density  $\rho = 7832.0$  kg/m<sup>3</sup>.

The clay soil materials are taken from the refuse dump landslide in the Jingxing dolomite mines, near Chongqing in China. The landslide mainly consists of silty clays. The natural mechanical parameters of silty clays are listed in Table 1. By using the soil compaction tests, it can be found that the optimum moisture content is 12.6% and the maximum dry density is 1.8 g/cm<sup>3</sup>. In the present experiments, in order to physically simulate the behavior of the actual sliding body, the screening experiments of natural silty clays are conducted after silty clays are crushed and dried. The results of screening experiments showed that quality distributions of dried silty clays in that 0.15–0.5, 0.05–0.15 and < 0.05 mm are 12, 34 and 54%, respectively. Then, the sliding mass is approximated by a mixture of uniform dried silty clays and water, mixed in proportions of 87.4 and 12.6%, respectively, while the silty clays at the compaction state are employed as sliding bed. Other mechanical parameters of sliding bed in the experimental model tests are listed in Table 2.

### Testing system

In the present physical landslide model test, strain gauges, which are XTR-2030 soil pressure cells, as shown in Figure S1b in the Supplementary Electronic Materials, are pasted on the h-type anti-sliding pile to measure the stress distribution. In addition, a DH3816 data collection system in Figure S1c is employed to collect the experimental data. The strain gauges are pasted on the front and back piles in an h-type anti-sliding piles. In the front pile, the spacing of strain gauges on the part between sliding surface and crossbeam is equal to 47.2 mm, and that of strain gauges on the cantilever

beam equates to 93.2 mm. While, in the back pile, the spacing of strain gauges on the part between sliding surface and crossbeam is 69.5 mm. In addition, the loading device consists a cushion block, a lever, a loading frame and standard blocks, as shown in Figure S1d. In the present experiments, magnitude of the static loads acting on the slope crest is equal to 18.09 kPa, which is equal to the bearing capacity of grounds in similar model tests (Zhao et al. 2017).

### Installation procedures of landslide models

The installation procedures of the physical landslide model tests are as follows:

1. The installation of sliding bed can be divided into several similar steps. The silty clay at compaction state is uniformly placed in the landslide model frame with 5 mm in height for one layer. After placing one layer of compact silty clay, this layer of compact silty clay is subjected to uniform static loads by the concrete block for 2 h. Repeat the above steps until the height of soil reaches 540 mm, as shown in Figure S2a.
2. It can be found from Figure S2b in the Supplementary Electronic Materials that a layer of polyethylene film is adopted as the sliding surface in the similar landslide model. In order to avoid the friction between soil and the model frame, two layers of polyethylene films are also attached to the inside surface of model frames.
3. The anchor depths are marked on the steel h-type anti-sliding piles. Moreover, strain gauges are placed on the h-type anti-sliding piles, as shown in Figure S2b-c. Then, the h-type anti-sliding piles are installed in the sliding bed with anchor depths of design.
4. In order to ensure the uniform characteristic of soil in sliding mass, the uniform mixtures of dried silty clay and water are layered in the landslide model frame with depth of 10 mm. After every layer of the uniform mixtures is placed into the landslide model frame, the mixture of soils should be rested for 2 h. When the height of sliding mass reaches 1000 mm, the sketch of sliding slope is created by the scratch tool, as shown in Figure S2d. Then, in order to ensure that the soil in the landslide model frame balances itself, the whole landslide model should be rested for 2 days.
5. The design loading schemes are exerted on the slope crest to model static loads of 18.09 kPa.

In order to investigate the anchor depths of h-type anti-sliding piles on deformation response and retaining mechanism in the clay landslides, four different landslide model tests are conducted. The geometrical conditions of h-type anti-sliding piles are listed in Table 3 based on the principles of similar model tests (Yang 2005) and previous works of

**Table 3** Geometrical sizes of the h-type anti-slide pile in the physical landslide model

No.	Length of cross-beam $L$ (mm)	Length of cantilever beam $H$ (mm)	Length of back pile $S_1$ (mm)	Length of front pile $S_2$ (mm)	Anchor depth $Z$ (mm)
1	250	250	256	189	88
2	250	250	256	189	132
3	250	250	256	189	176
4	250	250	256	189	220

anti-sliding piles by Zhao et al. (2017), Li et al. (2017), Tang et al. (2014) and Xiang et al. (2015). The installation procedures of landslide models containing h-type anti-sliding piles with different anchor depths are as same as the above descriptions.

**Numerical method**

ABAQUS is a three-dimensional explicit FEM for geotechnical engineering computations. It has been widely used in many geotechnical applications, such as mining engineering, tunnel engineering and slope engineering. Cheng and Jeremic (2009) investigated the behaviors of soil-pile-column system during liquefaction events, including lateral soil deformation, effects of pile pinning and ground settlement. Muraro et al. (2014) studied the stability and reliability of the ultimate limit state conditions of passive piles in frictional soils by a 3D-FEM model. Jamsawang et al. (2015) analyzed deformable characteristics and safety factors of the excavated slopes using 3D-FEM.

In the Supplementary Electronic Materials, Figure S3a-S3c illustrates the 3D discretization into finite elements using ABAQUS. It can be found from Figure S3b that three-dimensional eight-noded hexahedral elements (C3D8R) are used to simulate the h-type anti-sliding piles, whereas three-dimensional four-noded tetrahedral elements are applied to simulate soil in Figure S3c, which is considered as an elastoplastic Mohr–Coulomb model with non-associated flow rule. In order to simulate the soil-pile interactions, the fine three-dimensional four-noded solid elements (C3D4) are used in soils around the h-type anti-sliding piles to construct the surface-to-surface discretization. Surfaces of h-type anti-sliding piles are considered as “Master Surface,” and ones of soils round

h-type anti-sliding piles are considered as “Slave Surface.” In addition, “Hard” property is employed as the normal behaviors, and “Penalty function method” with Coulomb frictional law is used as the tangential behaviors in soil-pile interactions.

In the 3D numerical models, boundary conditions in the landslide model containing an h-type anti-sliding pile are described as follows: Six freedom degrees of nodes on the bottom surface of sliding beds are fixed. On the four side surfaces, displacements along the directions normal to surfaces are also fixed. In addition, the static loads are applied on the top surface of the present models.

In the experimental tests, h-type anti-sliding piles are hollow steel tubes. Due to solid elements used in the numerical simulations, the corrected mass density of piles in numerical simulations is listed in Table 4 by using the quality conversional method (Yang et al. 2006). Moreover, the corresponding Young’s modulus and flexural stiffness can be obtained by using the simple supported beam tests of the hollow steel tubes. The expression of Young’s modulus in the simple supported beam tests is expressed as follows:

$$E = \frac{Gl^3}{48If} \tag{1}$$

where  $E$  is correctional Young’s modulus with unit of kPa,  $G$  is the central load at the mid-span with unit of kN,  $l$  is the span of simply supported beam with unit of m,  $I$  is the second moment of area of simple supported beam with unit of  $m^4$  and  $f$  is mid-span deflection with unit of m. The correctional Young’s modulus in solid element of piles is also listed in Table 4. The mechanical parameters of soils in landslide models are same as the experimental tests, as shown in Table 4.

**Table 4** Mechanical parameters in numerical models

Model type	Density $\rho$ ( $kg/m^3$ )	Young’s modulus $E$ (MPa)	Poisson’s ratio $\nu$	Cohesive strength $c$ (kPa)	Internal frictional angle $\varphi$ ( $^\circ$ )
Anti-slide piles	832	43,400	0.2	–	–
Slide bed	1986	8	0.25	57.5	23.5
Slide mass	1850	6	0.3	48.6	19.8



### Experimental results

The experimental data of sliding thrust and resistant stresses are divided into two parts on the front pile and back pile, respectively.

The monitoring sliding thrust and resistant stresses on the front piles of h-type anti-sliding piles with different anchor depths in landslide model tests are, respectively, plotted in Fig. 2a, b. It can be observed from Fig. 2a that the sliding thrust stresses on the front piles are distributed in the trapezoid shapes. As anchor depths of h-type pile increase, the maximum values of sliding thrust stresses on the front piles gradually decrease, as shown in Fig. 2a. Moreover, it can be found from Fig. 2a that the location of maximum sliding thrust stress on the front pile is slightly less than 189 mm, which indicates that the maximum sliding thrust stress occurs below the crossbeam of the front pile. However, when the anchor depth of an h-type

anti-sliding pile is larger than 100 mm, the location of maximum sliding thrust stress on the front pile is above the crossbeam. Simultaneously, when anchor depth is larger than 100 mm, the distance between locations of the maximum sliding thrust stress on the front pile and sliding surfaces increases with the increase in anchor depth. Figure 2b shows that the distributions of resistant stresses on the front pile are in the approximate rectangular shape. When the anchor depth of an h-type anti-sliding pile increases, the resistant stresses on the front pile gradually increase, as shown in Fig. 2b.

Similarly, the distributions of monitoring sliding thrust and resistant stresses on the back piles of h-type anti-sliding piles with different anchor depths in landslide model tests are, respectively, plotted in Fig. 2c–d. It can be observed from Fig. 2c–d that distributions of sliding thrust and resistant stresses on the back pile in landslide models are in the triangular shapes. As shown in Fig. 2c, the sliding thrust stresses on the back piles decrease with the increase

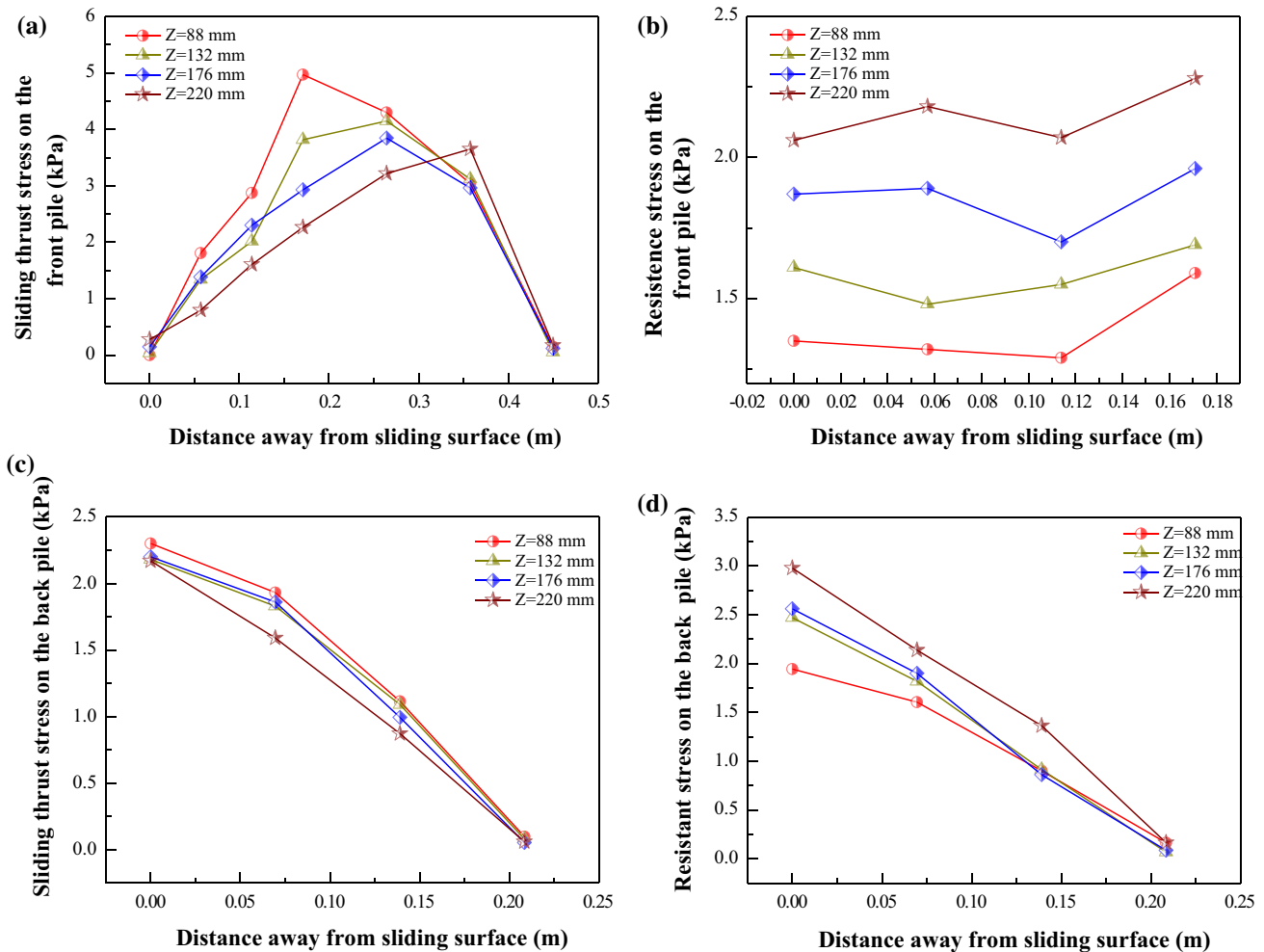


Fig. 2 Sliding thrust and resistant soil pressures on the a–b front and c–d back piles in h-type anti-sliding piles with different anchor depths in experiments

in anchor depth. In addition, it can be found from Fig. 2c that the resistant stresses on the back piles increases as the anchor depth increases. This phenomenon is induced by the larger contact area of back piles with deeper anchor depth.

Therefore, it can be indicated that distributions of sliding thrust stresses on the front and back piles of an h-type anti-sliding pile in a landslide model can be considered as trapezoid and triangular shapes, respectively, as shown in Fig. 2a, c, whereas it can be found from Fig. 2b, d that distributions of resistant stresses on the front and back piles of an h-type anti-sliding pile can be considered as rectangular and triangular shapes, respectively. The differences of sliding thrust and resistant stresses between front and back piles are induced by the typical structure of an h-type pile. The existence of crossbeam in h-type piles may change the stress states of back and front piles.

### Numerical results and discussions

#### Numerical results of the physical model tests

The numerical progresses can be divided into two parts: initial geostatic equilibrium state without an h-type anti-sliding

pile and loading state containing an h-type anti-sliding pile in landslide models. In this subsection, four existing physical similar model tests with detailed geometrical conditions in Table 3 are simulated using FEM. The four numerical models have same geometric parameters, i.e.,  $S_1$ ,  $S_2$ ,  $H$  and  $L$ , and different anchor depths  $Z$ .

Figure 3 shows the differences of Von Mises equivalent stress distributions in the numerical landslide models between the initial geostatic equilibrium state (left column) and loading state (right column) containing h-type anti-sliding piles. The corresponding Von Mises equivalent stress distributions in landslide models containing h-type anti-sliding piles with different anchor depths, i.e.,  $Z = 88$  mm,  $Z = 132$  mm,  $Z = 176$  mm and  $Z = 220$  mm, are plotted in Fig. 3a–d, respectively. It can be found from Fig. 3 that Von Mises equivalent stresses mainly concentrate on the sliding mass in the slopes before construction of h-type anti-sliding piles. The concentration of stresses on the sliding mass will cause landslides. While, after construction of h-type anti-sliding piles, Von Mises equivalent stresses mainly concentrate on the front piles of h-type anti-sliding piles, as shown in Fig. 3a–d. When anchor depth is smaller than 100mm, it can be found from Fig. 3a that the concentration of maximum Von Mises equivalent stress is located

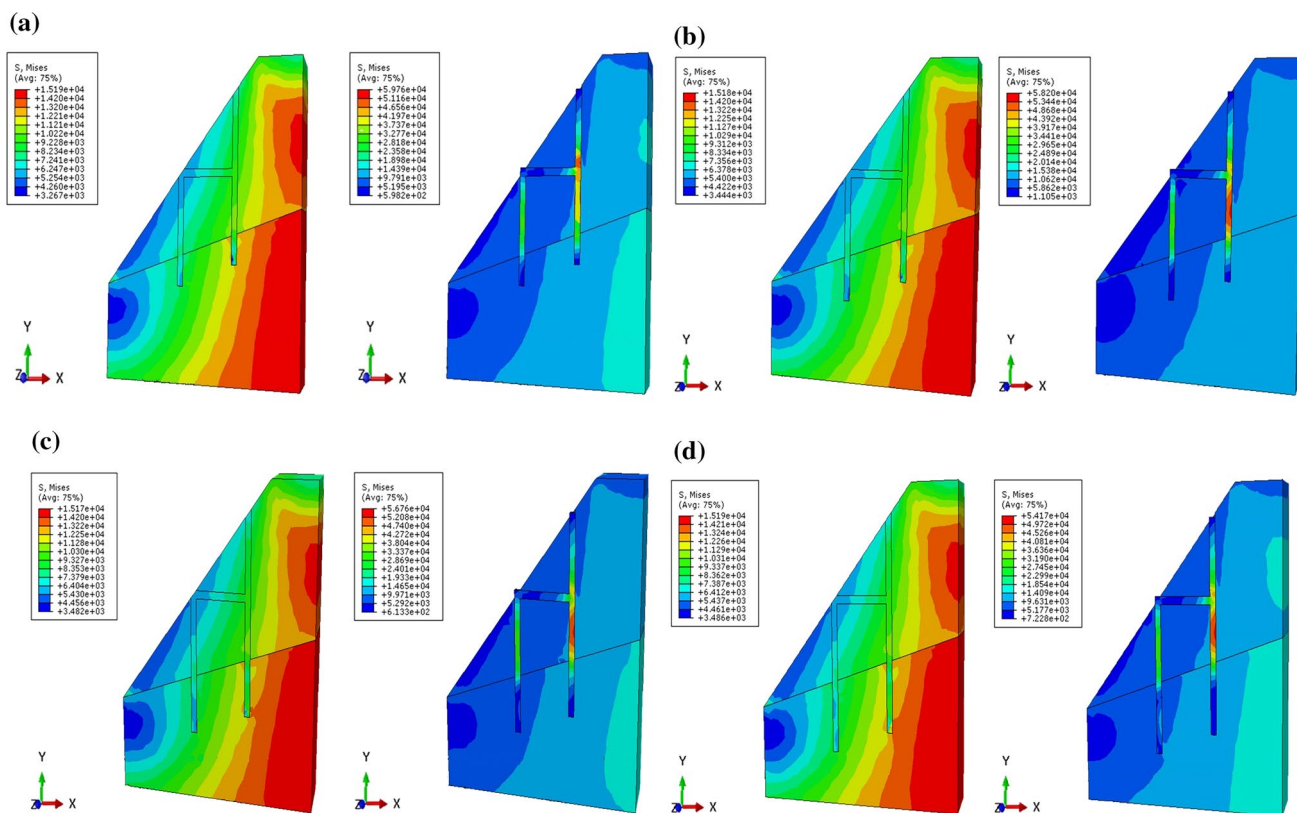


**Fig. 3** Von Mises equivalent stress contours of h-type anti-sliding piles with the fixed crossbeam length of  $L = 250$  mm and different anchor depths: **a**  $Z = 88$  mm, **b**  $Z = 132$  mm, **c**  $Z = 176$  mm and **d**  $Z = 220$  mm in landslide models with sliding surface angle of  $\alpha = 15^\circ$  (Unit: Pa)

on the front pile, which is slightly higher than one at cross-beam. As shown in Fig. 3b–d, when anchor depth is larger than 100mm, the maximum values of Von Mises equivalent stresses are located at the front piles, which are lower than the crossbeams and near the sliding surfaces. This phenomenon indicates that the h-type anti-sliding piles have the significant roles in terms of improve the stress states of slopes. Moreover, maximum values of Von Mises equivalent stresses increase with anchor depth increasing, as shown in Fig. 3.

The comparison of sliding thrust and resistant stresses on the front piles obtained from numerical simulations and experimental model tests are, respectively, shown in Fig. 4a, b. It can be found from Fig. 4 that the numerical results are in good agreement with the experimental data. As shown in Fig. 4a, the maximum value of sliding thrust stress decreases with anchor depth of the front and back piles increasing. Similarly, it can also be observed from Fig. 4b that the resistant stress increases as the anchor depth increases.

### Effect of sliding surface angles

In order to investigate the effect of sliding surface angle on deformation response and retaining mechanism of h-type anti-sliding piles in landslide models, four h-type anti-sliding piles with fixed anchor depth of  $Z = 220$  mm, cross-beam length of  $L = 200$  mm in landslide models with different sliding surface angles, i.e.,  $10^\circ$ ,  $15^\circ$ ,  $20^\circ$  and  $25^\circ$ , are simulated using ABAQUS, as shown in Fig. 1b. Moreover, mechanical parameters, boundary and loading conditions are the same as those described in “Numerical method” section.

In the Supplementary Electronic Materials, Figure S4 shows Von Mises equivalent stresses in four h-type anti-sliding piles with  $Z = 220$  mm,  $L = 200$  mm and various sliding surface angles, i.e.,  $10^\circ$ ,  $15^\circ$ ,  $20^\circ$  and  $25^\circ$ . It can be found from Figure S4 that when anchor depths and crossbeam lengths of h-type anti-sliding piles are fixed, sliding surface angle has an important influence on deformation response and retaining mechanism of h-type anti-sliding piles in landslide models. When sliding surface angle is less than  $20^\circ$ , stresses on the back piles are larger than those on the front piles, which indicates that the back piles play a main role in terms of retaining landslides. However, when sliding surface angle equates to  $25^\circ$ , stresses on the back piles are smaller than ones on the front piles, which illustrates that the front piles play a primary role in retaining landslides. Meanwhile, it can be found from Figure S4 that the maximum value of Von Mises equivalent stresses increases with sliding surface angle  $\alpha$  increasing.

The horizontal and vertical displacement contours of four h-type anti-sliding piles with different crossbeam lengths, which are magnified by 6000 times, are plotted in Figure S5 in the Supplementary Electronic Materials. It can be found from Figure S5 that when anchor depths and crossbeam lengths are fixed displacements and deformations of h-type anti-sliding piles increase as same as the maximum stresses with increasing sliding surface angles.

Sliding thrust and resistant stresses on the front and back piles are plotted in Fig. 5a, b, respectively. Figure 5a shows sliding thrust and resistant stresses on the front piles in landslide models with different sliding surface angles. It can be found from Fig. 5a that as the sliding surface angles  $\alpha$  increase, sliding thrust stresses on the front piles gradually

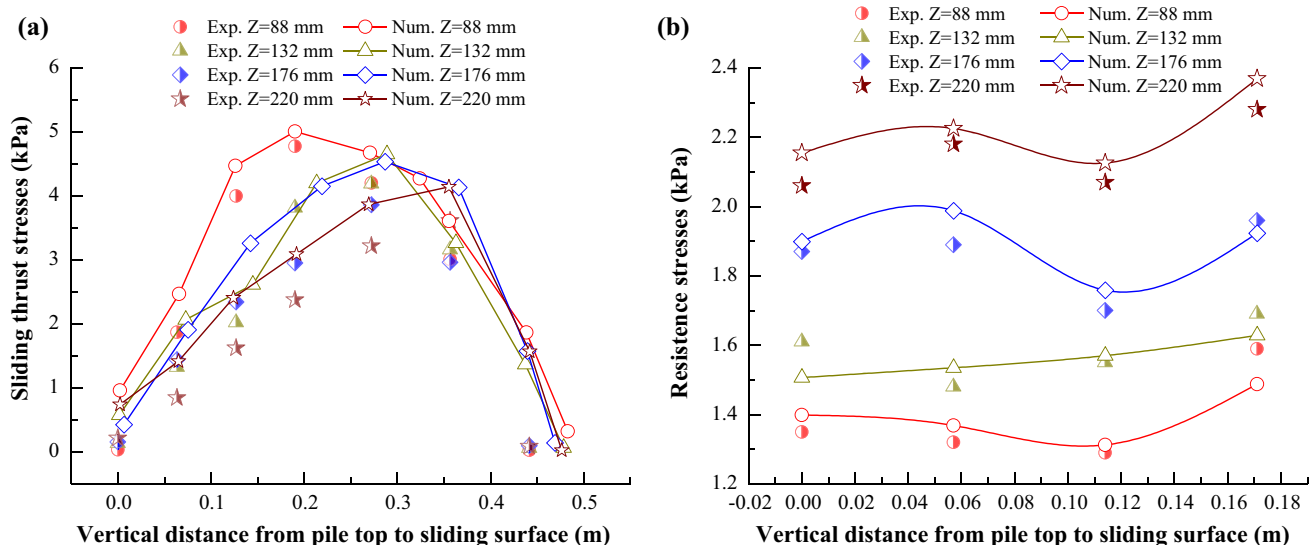
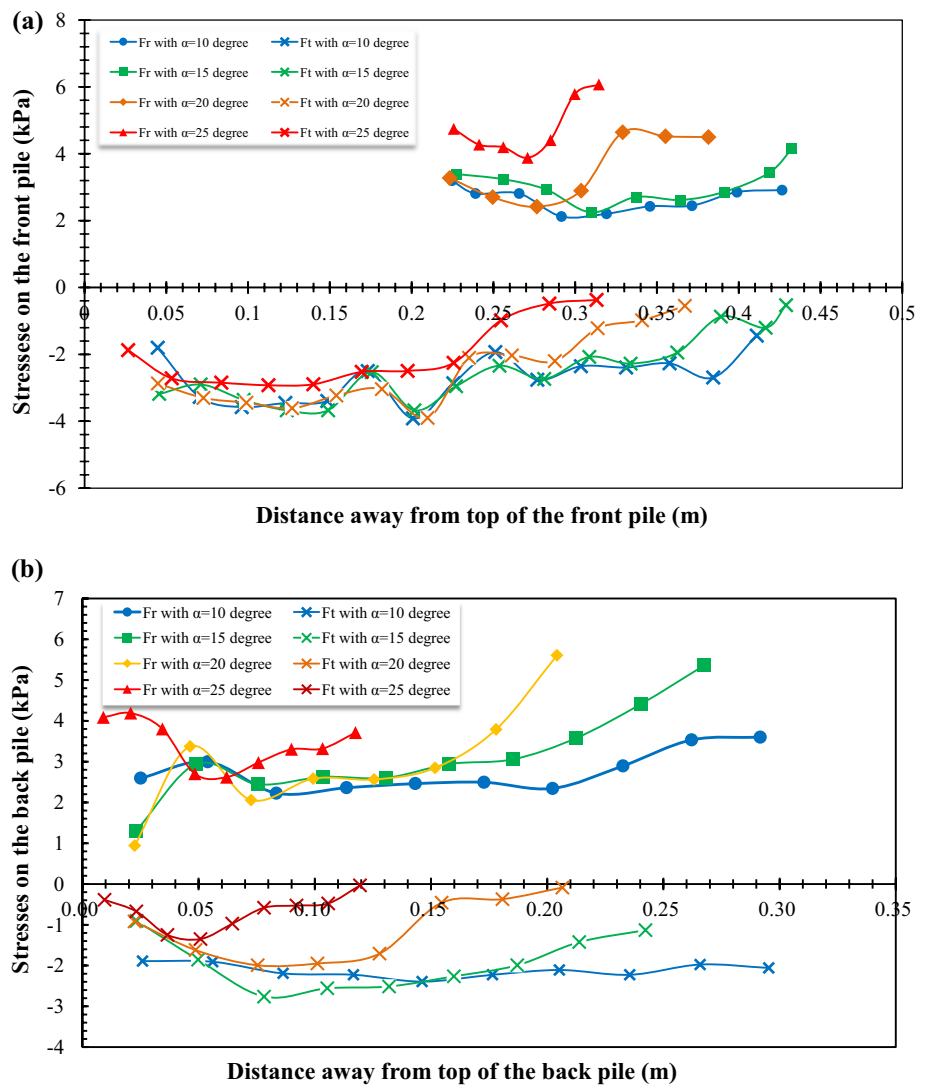


**Fig. 4** Comparison of the **a** sliding thrust stresses and **b** resistant stresses on the front pile between experimental data and numerical results in h-type anti-slide pile with different anchor depths



**Fig. 5** Numerical results of the sliding thrust and resistant pressures on **a** the front pile and **b** the back pile of h-type anti-sliding piles in landslide models with different sliding surface angles (Ft denotes the sliding thrust stress and Fr denotes the resistant stress)



decrease. However, the resistant stresses on the front pile increase with the increase in  $\alpha$ . It also can be found from Fig. 5a that sliding thrust stresses at top of front piles are larger than those at the bottom of front piles.

Figure 5b performs sliding thrust and resistant stresses on the back piles in landslide models with various  $\alpha$ . As shown in Fig. 5b, as sliding surface angle increases, distributions of sliding thrust stresses on the back pile convert from the approximately rectangular shapes ( $\alpha = 10^\circ$ ) to the triangular shapes, i.e.,  $\alpha = 15^\circ, 20^\circ$  and  $25^\circ$ . Moreover, when the sliding surface angles increase, sliding thrust stresses on the back piles gradually decrease, as shown in Fig. 5b. It also can be observed from Fig. 5b, resistant stresses on the back piles increase as the sliding surface angles increase. When the sliding surface angles  $\alpha = 10^\circ, 15^\circ$ , or  $20^\circ$  resistant stresses at the bottom of back piles are larger than those at the top of back piles. However, when the sliding surface angle  $\alpha = 25^\circ$ , resistant stresses at the top of back piles are larger than ones at the top of back piles, as shown in Fig. 5b.

### Effect of crossbeam length

In order to study effect of crossbeam length on deformation response and retaining mechanism on h-type anti-sliding piles, h-type anti-sliding piles with fixed anchor depth of  $Z = 220$  mm and sliding surface angle of  $\alpha = 10^\circ$  and  $20^\circ$  are simulated. The crossbeam lengths of h-type anti-sliding piles are, respectively,  $L = 100$  mm,  $L = 150$  mm,  $L = 200$  mm and  $L = 250$  mm, which are equal to 4 times, 6 times, 8 times, 10 times of pile size of 25 mm. The stiffness of crossbeam is denoted as 1.0 EI.

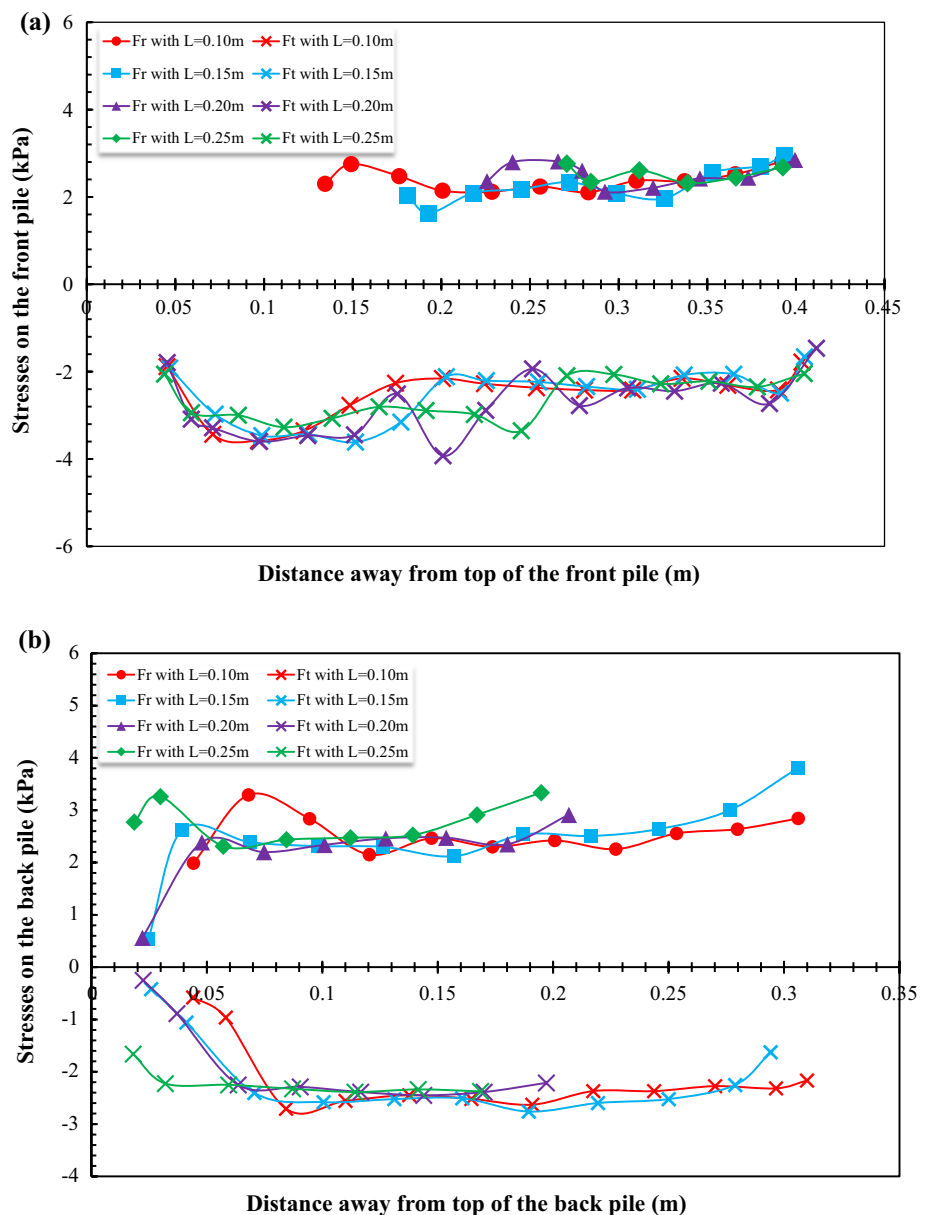
In Supplementary Electronic Materials, Figure S6a-S6d shows Von Mises equivalent stress contours of h-type anti-sliding piles with different crossbeam lengths in the landslide model containing sliding surface angle of  $\alpha = 10^\circ$ . It can be observed from Figure S6 that the maximum values of stresses are concentrated at the middle position of the back piles above sliding surfaces. This phenomenon indicates that the back pile plays a main retaining role of the

h-type anti-sliding pile in landslide model with  $\alpha = 10^\circ$ . Moreover, the maximum value of Von Mises equivalent stress decreases as crossbeam length in an h-type anti-sliding pile increases, as shown in Figure S6.

The horizontal displacement contours of four h-type anti-sliding piles with different crossbeam lengths, which are magnified by 6000 times, are plotted in Figure S7 in the Supplementary Electronic Materials. It can be observed from Figure S7 that when  $\alpha = 10^\circ$ , as crossbeam length increases, the horizontal displacements of h-type anti-slide piles decrease. The degree of pile deformation also reduces with the increase in crossbeam length. It indicates that retaining capability increases with crossbeam length increasing when sliding surface angle of  $10^\circ$ .

The relationship between sliding thrust and resistant stresses on the front and back piles of h-type anti-sliding piles with different crossbeam lengths in landslide models with  $\alpha = 10^\circ$  is shown in Fig. 6. For the front piles in h-type anti-sliding piles, sliding thrust and resistant stresses are distributed in the approximately rectangular shapes, as shown in Fig. 6a. It also can be found from Fig. 6a that as crossbeam length  $L$  increases, location of maximum sliding thrust stresses moves from positions near the top of piles toward ones near the sliding surfaces. For the back piles in h-type anti-sliding piles, as shown in Fig. 6b, sliding thrust and resistant stresses are distributed in the approximately rectangular shapes, and sliding thrust stresses near the top of back piles increase with crossbeam length increasing. In addition, it can be observed from Fig. 6b that as crossbeam

**Fig. 6** Numerical results of the sliding thrust pressure (Ft) and resistant pressure (Fr) on **a** the front pile and **b** the back pile with the fixed sliding surface angle of  $10^\circ$  and anchor depth of  $Z = 0.22$  m



lengths increase, resistant stresses at the bottom of back piles increase.

Similarly, Von Mises equivalent stress contours of h-type anti-sliding piles with different crossbeam lengths in the landslide models with sliding surface angle of  $\alpha = 20^\circ$  are plotted in Figure S8 in the Supplementary Electronic Materials, respectively. It can be found from Figure S8(a)–S8(c) that when crossbeam lengths are equal to 100, 150 and 200 mm the maximum values of Von Mises equivalent stresses are located at back piles. However, when crossbeam length equates to 250 mm, the maximum value of Von Mises equivalent stress is situated at the front back piles, as shown in Figure S8(d). This phenomenon indicates that the primary retaining role of h-type anti-sliding piles transforms from the back piles to the front piles, as crossbeam length in landslide model with  $\alpha = 20^\circ$  increases. It can be found from Figures S6 and S8 in the Supplementary Electronic Materials that location of the primary retaining role is not only related to the sliding surface angle, but also related to the crossbeam length of an h-type anti-sliding pile.

The horizontal displacement contours of four h-type anti-sliding piles with different crossbeam lengths, which are magnified by 6000 times, are plotted in Figure S9 in the Supplementary Electronic Materials. It can be found from Figure S9 that when  $\alpha = 20^\circ$ , as crossbeam length increases, horizontal displacement of h-type anti-slide piles grows. Meanwhile, the degree of pile deformation also grows with crossbeam length increasing, as shown in Figure S9. It indicates that retaining capability of deformations decreases as crossbeam length increases when sliding surface angle of  $20^\circ$ .

In Supplementary Electronic Materials, Figures S10a–S10b show the relationship between sliding thrust and resistant stresses on the front and back piles of h-type anti-sliding piles with different crossbeam lengths in landslide models with  $\alpha = 20^\circ$ , respectively. As shown in Figure S10a, sliding thrust stresses on the front piles are distributed in approximately trapezoidal shapes. Sliding thrust stresses near top of the front piles are independent of crossbeam lengths. Whereas, sliding thrust stresses near bottom of front piles increase with the growth of crossbeam length in h-type anti-sliding piles. The resistant stresses on the front piles are irregularly distributed, and resistant stresses on the front piles increase with crossbeam length increasing, as shown in Figure S10a.

As shown in Figure S10b, sliding thrust stresses on the back piles are distributed in approximately parabolic shapes. When crossbeam length is smaller than 250 mm, sliding thrust stresses near top of the back piles are independent of crossbeam lengths, as shown in Figure S10b. However, it can be found from Figure S10b that sliding thrust stresses near bottom of the back piles decrease with the increase in crossbeam length when  $L < 250$  mm. In addition, when

crossbeam length is smaller than  $L = 250$  mm, i.e., 10 times of pile size, resistant stresses near bottom of the back piles increase with crossbeam length increasing, as shown in Figure S10b. However, resistant stresses near top of the back piles are independent of crossbeam lengths.

In addition, in order to investigate the effect of pile sizes, four numerical h-type anti-sliding piles with different section stiffnesses, i.e., 1.0 EI, 1.5 EI, 2.0 EI and 2.5 EI, are simulated in numerical landslide models. In these four numerical models, crossbeam length, anchor depth and sliding surface angle are equal to 200, 220 mm and  $10^\circ$ , respectively. The other mechanical parameters, boundary and loading conditions are as same as those described in “Numerical method” section.

The sliding thrust and resistant stresses on the front piles of h-type anti-sliding piles in landslide models are depicted in Fig. 7a. Simultaneously, the associated sliding thrust and resistant stresses on the back piles of h-type anti-sliding piles in landslide models are plotted in Fig. 7b. As shown in Fig. 7, numerical results indicate that the section stiffness, i.e., pile size, has slight influence on the mechanical behaviors of h-type anti-sliding piles in landslide models.

### Effect of anchor depths in the front and back piles

In order to investigate the effect of anchor depths in the front and back piles on deformation response and retaining mechanism in h-type anti-sliding piles, two groups of numerical landslide models containing an h-type anti-sliding pile are simulated, as shown in Fig. 1c. Geometrical conditions for two groups of numerical samples have been plotted in Fig. 1c. The slope inclination angle and sliding surface angle in numerical samples are  $45^\circ$  and  $15^\circ$ , respectively.

As shown in Fig. 1c, there are two kinds of h-type anti-sliding piles in landslide models. In the first one, crossbeam length of h-type anti-sliding piles is equal to  $L = 200$  mm, the height of the front pile above the crossbeam equates to  $H = 200$  mm, and the anchor depth of back piles is fixed as  $Z = 220$  mm. In the second one, crossbeam length of h-type anti-sliding piles is equal to  $L = 250$  mm, the height of the front pile above the crossbeam equates to  $H = 250$  mm, and the anchor depth of back piles is fixed as  $Z = 220$  mm. It can be found from Fig. 1c that as the inclination angle between bottom of back pile and one of front pile is denoted as  $\theta$  (positive angle measured counterclockwise and negative angle measured clockwise). When the inclination angle varies from  $15^\circ$  to  $-30^\circ$  in  $15^\circ$  interval, anchor length of front piles gradually increases. The other mechanical, boundary and loading conditions are same as descriptions in “Numerical method” section.

In the Supplementary Electronic Materials, Figure S11 shows Von Mises equivalent stress contours of h-type anti-sliding piles with fixed crossbeam length of 200 mm,

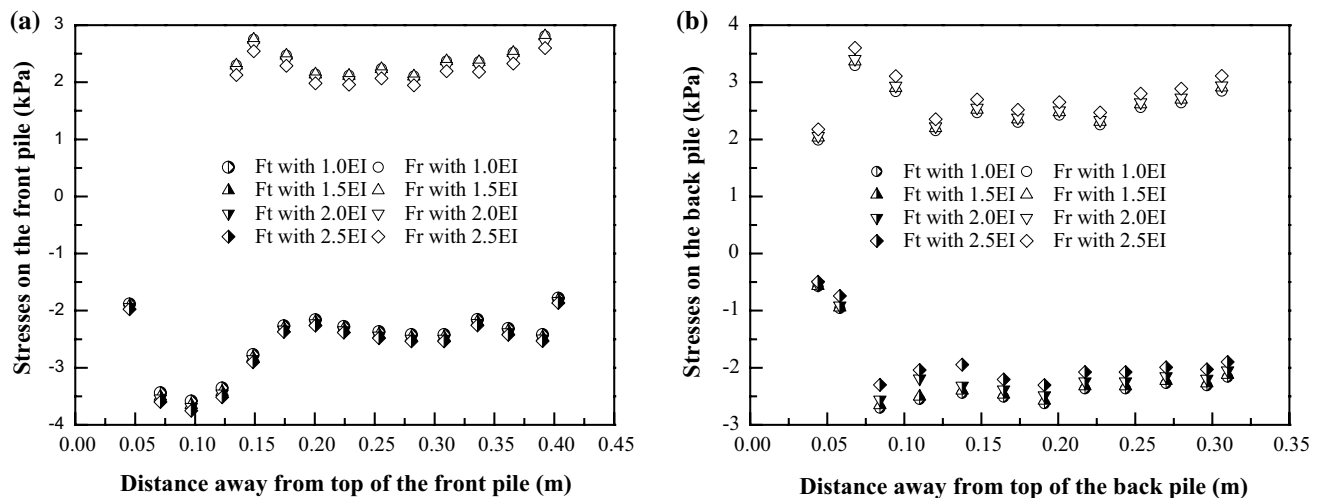


**Fig. 7** Influence of crossbeam stiffness on the sliding thrust stresses and resistant stresses on the **a** front and **b** back piles in a landslide model with sliding surface angle of  $10^\circ$  and anchor depth of  $Z = 0.22$  m

anchor depth of 220 mm and different inclination angle  $\theta$ . It can be found from Figure S11 that the maximum values of Von Mises equivalent stresses are located at the back piles in the interval between sliding surface and crossbeam.

In the Supplementary Electronic Materials, Figure S12 performs Von Mises equivalent stress contours of h-type anti-sliding piles with fixed crossbeam length of 250 mm, anchor depth of 220 mm and different inclination angle  $\theta$ . It can be found from Figure S12 that stresses on the front piles are larger than those on the back piles, which indicates that the front pile plays a main retaining role of the h-type anti-sliding pile in landslide model.

The relationships among inclination angle  $\theta$ , maximum values of Von Mises equivalent stress and horizontal displacement on h-type anti-sliding piles with  $L = H = 200$  mm are plotted in Fig. 8a. As shown in Fig. 8a, when anchor depths of front piles equate to ones of back piles, i.e.,  $\theta = 0^\circ$ , the maximum value of Von Mises equivalent stress in h-type anti-sliding piles is largest. However, when  $\theta = -15^\circ$ , the maximum value of Von Mises equivalent stress on h-type anti-sliding piles is smallest. Similarly, variation of inclination angle  $\theta$  and maximum value of horizontal displacements in h-type anti-sliding piles are also plotted in Fig. 8a. When  $\theta = 0^\circ$ , the horizontal displacement in an h-type anti-sliding pile is largest. However, as shown in Fig. 8a, when  $\theta = -15^\circ$ , the horizontal displacement in an h-type anti-sliding pile is smallest. Similarly, the maximum values of Von Mises equivalent stress and horizontal displacement on h-type anti-sliding piles with  $L = H = 250$  mm are depicted in Fig. 8b. It can be found from Fig. 8b that as the anchor depths of front piles increase, the horizontal displacement and stress in h-type anti-sliding piles decrease.

## Conclusions

In this paper, the deformation responses and retaining mechanism of h-type anti-sliding piles in landslide models are experimentally and numerically studied. In the experimental studies, four kinds of h-type anti-sliding piles with different anchor depths in landslide models are investigated. The experimental results show that distributions of sliding thrust stresses on the front and back piles of an h-type anti-sliding pile can be considered as trapezoid and triangular shapes, respectively. Whereas, the distributions of resistant stresses on the front and back piles of an h-type anti-sliding pile can be considered as rectangular and triangular shapes, respectively. As the anchor depth of an h-type anti-sliding pile increases, the sliding thrust stresses on piles decrease, but the resistant stresses on the front pile gradually increase.

The experimental examples are firstly simulated using FEM. The present numerical results are in good agreement with the experimental data. Then, effects of sliding surface angles, crossbeam lengths and different anchor depths on the deformation response and retaining mechanism of h-type anti-slide piles in landslide models are numerically studied. It can be found from numerical results that deformation responses and retaining mechanism of h-type anti-sliding piles are not only related to sliding surface angles, but also related to crossbeam length and anchor depths. Finally, based on the experimental and numerical results, some suggestions of designing h-type anti-sliding piles in slopes are proposed as follows.

1. Crossbeam length plays a significantly important role in the deformation response and retaining mechanism of h-type anti-sliding piles in landslides. While, the section

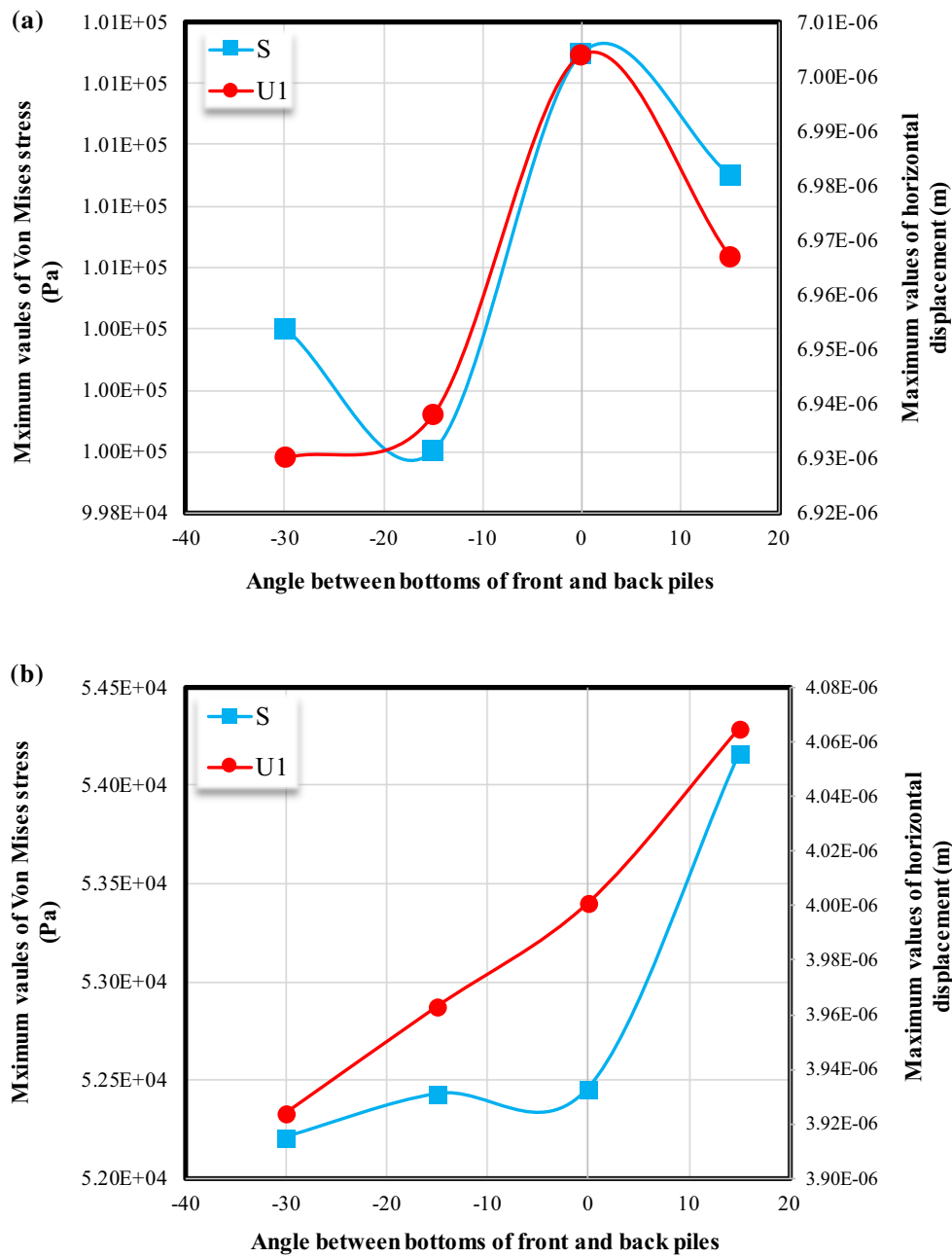


**Fig. 8** The effect of inclination angle  $\theta$  on the maximum values of horizontal displacement and Von Mises equivalent stress on h-type anti-sliding piles. **a**  $L = H = 200\text{mm}$  and **b**  $L = H = 250\text{mm}$  in landslide models

- stiffness of crossbeam in an h-type anti-sliding pile only slightly affects the deformation response and retaining mechanism of h-type anti-sliding piles in landslides.
- When sliding surface angle is small (around  $\alpha = 10^\circ$ ), crossbeam length is suggested to be equal to  $8 \sim 10$  times of pile size.
  - When sliding surface angle is large (around  $\alpha = 20^\circ$ ), crossbeam length is suggested to be equal to  $4 \sim 6$  times of pile size.

- The anchor depths of the front piles are suggested to be larger than those of the back piles in some degree, i.e., inclination angle  $\theta$  is around  $-15^\circ$ .

**Acknowledgements** The authors acknowledge the financial support provided by the National Natural Science Foundation of China (Nos. 41772319, 41372356 and 50104013).



## References

- Abramson LW, Thomas SL, Sunil S, Glenn MB (2002) Slope stability and stabilization methods. Wiley, New York
- Cheng Z, Jeremic B (2009) Numerical modeling and simulation of pile in liquefiable soil. *Soil Dyn Earthq Eng* 29(11–12):1405–1416
- Cornforth DH (2005) Landslides in practice. Wiley, New York
- Dai ZH (2002) Study on distribution laws of landslide-thrust and resistance of sliding mass acting on antislides piles. *Chin J Rock Mech Eng* 21(4):517–521
- Hassiotis S, Chameau JL, Gunaratne M (1997) Design method for stabilization of slopes with piles. *J Geotech Geoenviron* 123(4):314–322
- Ito T, Matsui T (1975) Methods to estimate lateral force acting on stabilizing piles. *Soils Found* 15(4):43–59
- Ito T, Matsui T, Pyo H, Wong WP (1981) Design method for stabilizing piles against landslide: one row of piles. *Soils Found* 21(1):21–37
- Jamsawang P, Voottipruex P, Boathong P, Mairaing W, Horpibulsuk S (2015) Three-dimensional numerical investigation on lateral movement and factor of safety of slopes stabilized with deep cement mixing column rows. *Eng Geol* 188:159–167
- Jiao YY, Wang ZH, Wang XZ, Adoko AC, Yang ZX (2013) Stability assessment of an ancient landslide crossed by two coal mine tunnels. *Eng Geol* 159:36–44
- Kim BT, Kim YS (1999) Back analysis for prediction and behavior of laterally loaded single piles in sand. *KSCE J Civ Eng* 3(3):272–288
- Kourkoulis R, Gelagoti F, Anastasopoulos I, Gazetas G (2011) Slope stabilizing piles and pile-groups: parametric study and design insights. *J Geotech Geoenviron* 137(7):63–677
- Li C, Tang H, Hu X, Wang L (2013) Numerical modelling study of the load sharing law of anti-sliding piles based on the soil arching effect for Erliban landslide, China. *KSCE J Civ Eng* 17(6):1251–1262
- Li C, Wang X, Tang H, Lei G, Yan J, Zhang Y (2017) A preliminary study on the location of the stabilizing piles for colluvial landslides with interbedding hard and soft bedrocks. *Eng Geol* 224:15–28
- Liu GD, Yu JM (1984) The measurement of the thrust of the landslide and its change regularities. In: *Proceedings of the Landslides*, vol 6, pp 105–115. China Railway Publishing House, Beijing
- Muraro S, Madaschi A, Gajo A (2014) On the reliability of 3D numerical analyses on passive piles used for slope stabilisation in frictional soils. *Géotechnique* 64(6):486–492
- Ou XD, Tang YC, Cui W, Li JQ, Pan X (2012) Model test and numerical simulation of h-shaped anti-sliding pile. *Chin J Rock Mech Eng* 39(1):1936–1943
- Poulos HG (1995) Design of reinforcing piles to increase slope stability. *Can Geotech J* 32(5):800–818
- Song YS, Hong WP, Woo KS (2012) Behavior and analysis of supporting piles installed in a cut slope during heavy rainfall. *Eng Geol* 129–130(12):56–67
- Tang H, Hu X, Xu C, Li C, Yong R, Wang L (2014) A novel approach for determining landslide pushing force based on landslide-pile interactions. *Eng Geol* 182:15–24
- Usluogullari OF, Temugan A, Duman ES (2016) Comparison of slope stabilization methods by three-dimensional finite element analysis. *Nat Hazards* 81(2):1027–1050
- Wang Y (2011) Calculation theory and design method research on h-type of anti-sliding piles. PhD Thesis. Chengdu University of Technology, Chengdu, China (in Chinese)
- Wang ZH, Zhou J (2011) Three-dimensional numerical simulation and earth pressure analysis on double-row piles with consideration of spatial effects. *J Zhejiang Univ Sci A Appl Phys Eng* 12(10):758–770
- Wang PY, Peng YQ, Liu YX (2010) Distribution of landslide thrust on anti-slide pile ascertained by specified shear opening method. *J Logist Eng Univ* 26(2):1–4
- Xiang B, Zhang LM, Zhou LR, He YY, Zhu L (2015) Field lateral load tests on slope-stabilization grouted pipe pile groups. *J Geotech Geoenviron* 141(1):04014124
- Xiao SG (2010) Approximate theoretical solution of distribution modes of landslide thrust on anti-sliding piles in soil-like slopes or landslides. *Chin J Geotech Eng* 32(1):120–123
- Xiong ZW (2000) Force distribution rule of deeply buried anti-slide pile. *China Rail Sci* 21(1):48–51
- Xu LD, Yin DC, Liu HM (1988) The distribution of resisting forces along piles in bulk medium slide. In: *Proceedings of the landslides*, vol 6, pp 84–91. China Railway Publishing House, Beijing
- Xu LD, Yin DC, Liu HM (1990) The resistance distribution in the slide mass of clayey soil in front of anti-sliding pile. In: *Proceedings of the landslides*, vol 6, pp 92–99. China Railway Publishing House, Beijing
- Yang JJ (2005) Similarity theory and structural model test. Wuhan University of Technology Press, Wuhan
- Yang T, Zhou DP, Zhang JY (2006) Distribution of land-slide thrust on anti-slide piles. *Chin J Geotech Eng* 28(3):322–326
- Zhao B, Wang YS, Wang Y, Shen T, Zhai YC (2017) Retaining mechanism and structural characteristics of h type anti-slide pile (hTP pile) and experience with its engineering application. *Eng Geol* 222:29–37
- Zheng YR, Zhao SY (2004) Application of strength reduction FEM in soil and rock slope. *J Rock Mech Geotech Eng* 23(19):3381–3388